**Didar K. YESKERMESSOV*, Sergey V. PLOTNIKOV*, Nazgul K. YERDYBAEVA***

# STRUCTURE AND PROPERTIES OF MULTI COMPONENT (Ti-Zr-Cr-Nb)N COATINGS OBTAINED BY VACUUM-ARC DEPOSITION

## STRUKTURA I WŁAŚCIWOŚCI WIELOSKŁADNIKOWYCH POWŁOK (Ti-Zr-Cr-Nb)N OTRZYMANYCH METODĄ ŁUKOWO-PRÓŻNIOWĄ

**Key words:**

multielement nitride, crystal structure, XRD, mechanical and tribological properties

**Słowa kluczowe:**

wieloskładnikowa powłoka azotowa, struktura krystaliczna, XRD, właściwości mechaniczne i tribologiczne

**Abstract**

Investigated multicomponent coating nitride (Ti-Zr-Cr-Nb)N in this study were obtained using a well-developed technique of vacuum-arc deposition. Theoretical and experimental studies show that the chemical composition, microstructure, and mechanical properties of coatings are based closely on

* D. Serikbayev East Kazakhstan State Technical University, 19 Serikbayev Street, Ust-Kamenogorsk, Kazakhstan, e-mail: didar.eskermesov@mail.ru.

deposition parameters (the working gas pressure and bias potential on the substrate). The microstructure and mechanical properties (Ti-Zr-Cr-Nb)N coatings were investigated using a scanning electron microscope (SEM) equipped with energy dispersive microanalysis prefix and X-ray diffraction (XRD). Phase analysis of nitride coatings (Zr-Ti-Cr-Nb)N indicates a TiN phase, $NbTiN_2$, ZrTiNb, ZrNb, TiCr and α-Ti. The coatings thickness reached 6.8 μm and their maximum of hardness was H = 43,7GPa. Tribological (test "ball-on-disc") and mechanical (scratch test) properties of multi-coating were studied. The experimental results obtained by studying multicomponent coatings (Ti-Zr-Cr-Nb)N are promising and can be used as protective coatings for cutting tools and structural materials.

## INTRODUCTION

The most promising and developing way to increase the efficiency of working surfaces of products is the formation ion-plasma coatings based on nitrides and carbides of refractory elements on tools and wear-resistant structural materials **[L. 1–8]**. However, during the study, we found that they have a number of drawbacks that limit the prospect of their use in industry. They have poor thermal shock resistance **[L. 2]**. When heating an example of the most common TiN-coated product above 400–500°C **[L. 9–12]** on the surface of the coating begins to grow brittle with a low adhesion layer of titanium oxide, which rapidly destroys the protective resistance of the coating. The mechanical and tribological properties of the coating are no longer sufficient.

In the last decade, there has been wide application multi-element coatings obtained with three-(Ti-Nb-N, Ti-Cr-N, Zr-Ti-N), the four-(Zr-Ti-Si-N), or a five- (Zr-Nb-Ti-Cr-N) of component systems. The structure properties, and the possibility of a thermal stabilization phase composition of alloy condensates have been little studied. The stability of the structure and composition, as well as high performance systems provide a multi-element nitride improve the physical and mechanical characteristics of the surface, and they can be used as protective films that prevent harmful impurities in the surface layers of the products. Studies of complex mechanical and physical properties of pure metals, such as zirconium, niobium, titanium, molybdenum, chromium, suggest the advisability of a vacuum plasma condensates based system Ti-Zr-Cr-Nb. This in turn creates a protective layer (or coating) based on of four items (four transition metals, and nitrogen, as part of the binder). Among the existing technologies such coatings are the most promising advanced vacuum ion-plasma methods. These techniques affect the formation of the structure and phase composition of the coatings. During deposition, it is also possible to form an amorphous structure, a decrease in grain size, obtaining new chemical compounds, can significantly improve their physical-mechanical properties.

Therefore, an actual problem is currently the application of methods for ion-plasma deposition to obtain multicomponent coatings based on (Ti-Zr-Cr-Nb)N. The purpose of this work is to study patterns of structures of multicomponent systems based coatings (Ti-Zr-Cr-Nb)N, and the study of their physical and mechanical properties.

## Equipment and methods

As a method of producing coating systems (Ti-Zr-Cr-Nb)N was applied by vacuum-arc deposition. Vaporized material is a cast cathode Ti + Zr + Cr + Nb composition: Ti – 12.32%, Zr – 27.99%, Cr – 37.39%, and Nb – 22.30%. The cathode is made by electron-beam melting. The coatings were deposited in the setting "Bulat-6", with-, a medium molecular nitrogen $N_2$ on the polished surface of the substrate 36 steel grade A570. Spray coating was carried out at a working gas pressure of 0.3 - 0.7 Pa. Potential bias was varied from -100 to -200 V. The substrates were heated to 450°C prior to the deposition. The distance between the substrates and the cathode was 250 mm. The coating thickness (Ti-Zr-Cr-Nb) N was 6.2–6.8 microns. The coating deposition parameters (Ti-Zr-Cr-Nb) N are shown in **Table 1**. A schematic diagram of vacuum-arc upgraded installation is shown in **Figure 1**.

The thickness of the coating, the condition of the boundaries between the base (substrate), and coating and surface morphology were studied using a scanning electron microscope scanning «JSM-6390LV» (Japan) with an accelerating voltage of 20–30 kV. The elemental composition of the coatings was analysed by an X-ray spectra characteristic with the built-in microscope "INSA Energy OXFORD» System X-ray energy dispersive spectrometer (UK).

X-ray diffraction analysis was carried out by analysing the diffraction patterns of the samples obtained on a diffractometer «Shimadzu XRD-7000S» (Japan). Diffraction patterns were recorded using $CuK_{\alpha 1/\alpha 2}$ radiation. The

**Table 1. Process of deposition parameters (Ti-Zr-Cr-Nb)N**
Tabela 1. Parametry procesu osadzania powłok (Ti-Zr-Cr-Nb)N

| № (series) | Deposited material | Arc current, $I_d$, A | Nitrogen pressure, $P_N$, Pa | Bias voltage, $U_{sm}$, V |
|---|---|---|---|---|
| 1 | (Ti-Zr-Cr-Nb)N | 110 | 0.3 | -100 |
| 2 | | | 0.7 | -100 |
| 3 | | | 0.3 | -200 |
| 4 | | | 0.7 | -200 |

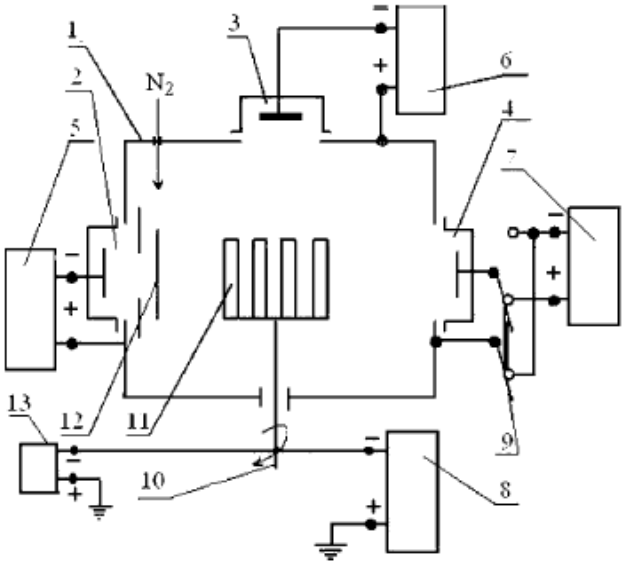


**Fig. 1. Schematic diagram of vacuum-arc deposition device. 1 - vacuum chamber; 2 , 3 , 4 – vacuum-arc evaporators; 5 , 6, 7 – evaporator power sources; 8 – power supply substrate; 9 – the switch; 10 – rotary device; 11 – processed products; 12 – the screen; 13 – high-voltage pulse generator**

Rys. 1. Schemat urządzenia dla metody łukowo-próżniowej (1 – komora próżniowa, 2, 3, 4 – katody, 5, 6, 7 – źródła energii elektrycznej zasilające katody, 8 – źródło zasilania energią podłoża, 9 – włącznik, 11 – elementy obrabiane, 12 – ekran, 13 – generator impulsów wysokiego napięcia

following parameters were used during the experiment: scan speed - 2º per minute – 0,03º – scanning step and a 10–90º range of angles, and an accumulation at 1.5 seconds. The average crystallite size was determined using the Debye-Scherrer equation from the broadening of the diffraction peaks, taking into account the instrumental broadening and software «PowderCell 2.4». The instrumental broadening was determined on the half-width of a standard silicon powder and the maximum was 0.14.

The analysis of surface roughness and morphology, as well as the amount of material removed was determined by coating the wear track cross-section on the surface of the sample by an automated contactless profilometer model «Micro Measure 3D Station» ( France) .

Microhardness measurements were performed on an automated hardness tester model «Durascan-20" (Switzerland) with a load on the indenter of 0.05 N and the nanohardness and elastic modulus were investigated under dynamic conditions on nanohardness «NANO Hardness Tester» (Switzerland). Imprints were made at a distance of 1.0 mm from each other. Each sample was held for 10 measurements. Components were polished prior to surface roughness

measurements to improve accuracy. Adhesion-cohesion strength, scratch resistance and coating failure mechanisms were studied in air using a scratch tester «Micro-Scratch Tester» (Switzerland). Scratches were made on the coatings with continuously increasing load values of the Rockwell C diamond indentor with a spherical radius of curvature of 100 micrometres and the parameters such as acoustic emission, the friction coefficient of the indenter, and the penetration depth were registered. The following basic critical loads for changing the coefficient of friction curves and acoustic emission load were fixed: $L_{c1}$ – characterizes the time of occurrence of the first chevron cracks, $L_{c2}$ – the time of occurrence of chevron cracks, $L_{c3}$ – destruction is cohesively-adhesive character, $L_{c4}$ – local exfoliation of the coating areas, and $L_{c5}$ – plastic abrasion coating to the substrate.

The tribological tests were performed in air on a "ball-on-disc" tester «PC-Operated High Temperature Tribometer» ( Switzerland). The counterface was a ball with a diameter of 3.0mm-, made of certified sintered material - $Al_2O_3$. The load was 5.0N, and the sliding speed was 2.5cm/s. Test conditions meet international standards ASTM G99 and DIN50324.

## RESULTS AND DISCUSSION

The research results of the elemental composition based on coatings systems (Ti-Zr-Cr-Nb)N, depending on the physical – technological deposition parameters are given in **Table 2**.

**Table 2. The results of the energy dispersive analysis of coating systems (Ti-Zr-Cr-Nb)N**
Tabela 2. Wyniki analizy dyspersji energii w systemach powłokowych (Ti-Zr-Cr-Nb)N

| Number of series | Elemental composition of the coatings at. % | | | |
|---|---|---|---|---|
| | Ti | Zr | Cr | Nb |
| | The elemental composition of the cathode before deposition | | | |
| | 12.32 | 27.99 | 37.39 | 22.30 |
| 1 | 13.47 | 27.87 | 14.89 | 43.77 |
| 2 | 12.07 | 23.55 | 14.82 | 49.56 |
| 3 | 25.73 | 18.54 | 36.95 | 18.78 |
| 4 | 28.15 | 20.74 | 31.27 | 19.84 |

According to the results of scanning electron microscopy, vacuum- arc condensation of a multi-component system has a number of features in the formation of the surface morphology. **Figure 2** shows the SEM image of one of the resulting coating system (Ti-Zr-Cr-Nb)N.

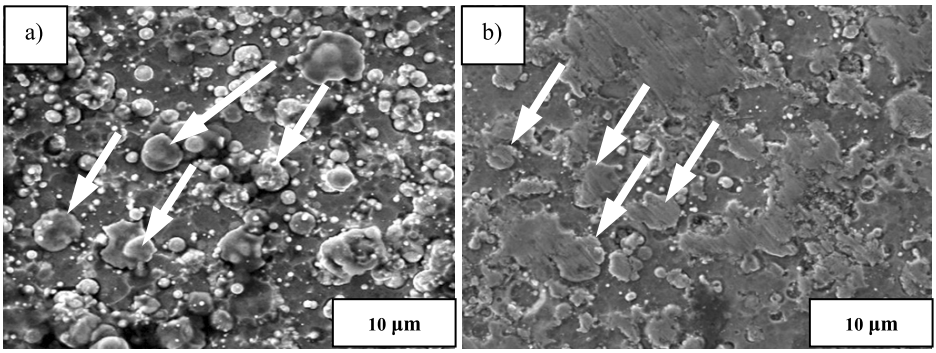


**Fig. 2. SEM image of the surface coating (Ti-Zr-Cr-Nb)N: ($P_N$ = 0.3 Pa, U = -100 V); b) ($P_N$ = 0.7 Pa, U = -200 V)**

Rys. 2. Zdjęcia mikroskopowe SEM powierzchni powłoki (Ti-Zr-Cr-Nb)N: ($P_N$ = 0,3 Pa, U = -100 V); b) ($P_N$ = 0,7 Pa, U = -200 V)

The main difference of the vacuum arc deposition, in particular, in operation of the cathode spot of the arc, is the production of molten droplets, which can be incorporated into the coating in the form of microparticles. As seen in **Figure 2a**, coating (Ti-Zr-Cr-Nb)N contains inclusions of droplet fractions of various sizes (up to 8 mm in diameter). In this case, the microdroplets are in the form of an ellipsoid, which indicates that the droplets fly almost parallel to the substrate plane. Raising the deposition temperature using the flow bias (U = -200 V) significantly reduces the concentration of drops on the surface fraction **(Fig. 2b)**. Reduced droplet content can occur by melting the surface of the coating process.

RBS analysis results of the elemental composition of the coating (Ti-Zr-Cr-Nb)N are shown in **Figure 3**. As can be seen from the depth profiles of the elemental composition, the surface layer is enriched with atoms of N and Ti. Furthermore, the concentration of each constituent element is kept roughly constant with depth, indicating uniformity of the coating composition across the layer thickness. It should be noted that the (Zr-Ti-Cr-Nb)N coatings contain a small amount of oxygen and carbon.

**Figure 4** shows the X-ray diffraction spectra of the coatings. The results of the structural state of the resulting coatings are shown in **Tables 3** and **4**. As shown in **Table 3**, with increasing values of the bias potential applied to the substrate, there is an increase in crystallite size (L) of the TiN main phase.

Analysis of **Table 3** indicates a significant dependence between the coating composition and the bias potential applied to the substrate. An increase in the bias potential energy of the incident particle leads to a higher radiation component in the formation of coating patterns. Thus, increasing the bias potential to -200 leads to an increase in the content of strong nitride-forming components Ti, Nb, Cr, and Zr.

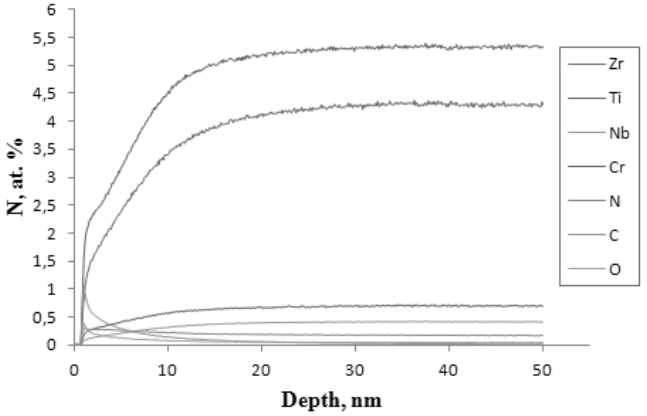


**Fig. 3. Elemental analysis of coating (Ti-Zr-Cr-Nb)N vs. depth ($P_N$ = 0.3 Pa , U = -200 V)**

Rys. 3. Analiza pierwiastków w funkcji głębokości dla powłoki (Ti-Zr-Cr-Nb)N ($P_N$ = 0,3 Pa, U = -200 V)

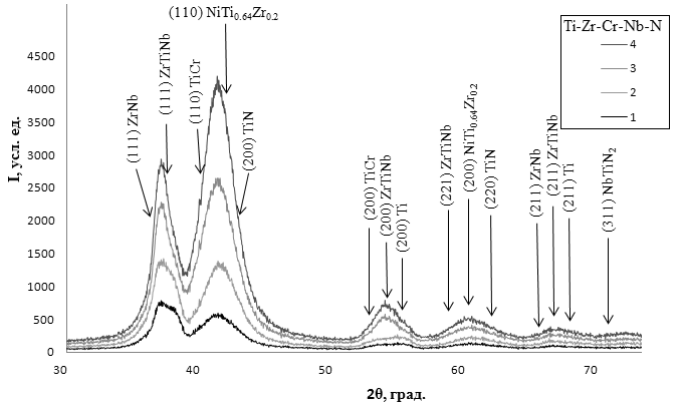


**Fig. 4. X-Ray patterns of coatings (Ti-Zr-Cr-Nb) N, obtained by different values of U and $P_N$ (the diagrams for conditions is presented in Table 1)**

Rys. 4. Dyfraktogramy rentgenowskie powłok (Ti-Zr-Cr-Nb) otrzymanych dla różnych wartości U i $P_N$ (wykresy dla danych przedstawionych w **Tabeli 1**)

**Table 3. Crystallite size (L) and the lattice constant (a) single phase TiN, coating systems based on (Ti-Zr-Cr-Nb)N**

Tabela 3. Wielkość krystalitu (L) i stała sieci (a) pojedynczej fazy TiN, w systemach powłokowych na bazie (Ti-Zr-Cr-Nb) N

| Parameters | Number of samples | | | |
|---|---|---|---|---|
| | 1 | 2 | 3 | 4 |
| *L*, nm | 8.06 | 8.06 | 11.16 | 14.80 |
| *a*, Å | 4.2434 | 4.2391 | 4.1993 | 4.2218 |

Phase analysis of nitride coatings (Zr-Ti-Cr-Nb)N indicates a TiN phase, $NbTiN_2$, ZrTiNb, ZrNb, TiCr and α-Ti. This included a $NiTi_{0.64}Zr_{0.2}$ phase. This is connected with the substrate, because the substrate composition includes Ni. In the deposition, the surface of the substrate is heated to the melting point of Ni, and there is a bonding with precipitating elements Ti and Zr to form a new phase.

**Table 4. Results of X-ray studies of coatings based on (Ti-Zr-Cr-Nb)N systems**
Tabela 4. Wyniki badań rentgenowskich systemów powłokowych na bazie (Ti-Zr-Cr-Nb) N

| Name of samples (series) | Phase detection | The content of the phase, volume . % | The lattice parameters | The crystallite size for OCD nm | Microstress |
|---|---|---|---|---|---|
| 1 | 2 | 3 | 4 | 5 | 6 |
| 1 | $NiTi_{0.64}Zr_{0.2}$ | 7.62 | a=3.0412 | 7.83 | 0.006027 |
| | TiN | 57.70 | a=4.2434 | 8.06 | 0.006234 |
| | ZrTiNb | 5.21 | a=3.3696 | 13.22 | 0.003221 |
| | ZrNb | 2.00 | a=3.4225 | 20.42 | 0.004669 |
| | $NbTiN_2$ | 1.50 | a=4.3401 | 13.22 | 0.001671 |
| | TiCr | 9.82 | a=3.1220 | 7.74 | 0.005611 |
| | Ti | 16.14 | a=3.2989 | 10.43 | 0.004045 |
| 2 | $NiTi_{0.64}Zr_{0.2}$ | 10.93 | a=3.0468 | 7.84 | 0.006041 |
| | TiN | 60.27 | a=4.2391 | 8.06 | 0.006226 |
| | ZrTiNb | 4.64 | a=3.3702 | 11.37 | 0.003248 |
| | ZrNb | 2.79 | a=3.4382 | 12.56 | 0.003042 |
| | $NbTiN_2$ | 2.15 | a=4.3376 | 16.56 | 0.000421 |
| | TiCr | 14.54 | a=3.1263 | 8.56 | 0.006011 |
| | Ti | 4.68 | a=3.3074 | 11.54 | 0.003011 |
| 3 | $NiTi_{0.64}Zr_{0.2}$ | 20.28 | a=3.0439 | 9.30 | 0.006393 |
| | TiN | 39.63 | a=4.1993 | 11.16 | 0.006094 |
| | ZrTiNb | 4.24 | a=3.3736 | 14.46 | 0.001986 |
| | ZrNb | 1.29 | a=3.4152 | 26.22 | 0.002938 |
| | 2 | 3 | 4 | 5 | 6 |
| | $NbTiN_2$ | 0.54 | a=4.3308 | 26.09 | 0.001288 |
| | TiCr | 25.33 | a=3.1281 | 7.75 | 0.005627 |
| | Ti | 8.70 | a=3.2670 | 7.92 | 0.005985 |
| 4 | $NiTi_{0.64}Zr_{0.2}$ | 24.72 | a=3.0569 | 8.36 | 0.005529 |
| | TiN | 44.28 | a=4.2218 | 14.80 | 0.004635 |
| | ZrTiNb | 3.56 | a=3.3772 | 12.09 | 0.002732 |
| | ZrNb | 1.58 | a=3.4243 | 15.12 | 0.002455 |
| | $NbTiN_2$ | 5.27 | a=4.4277 | 8.23 | 0.006551 |
| | TiCr | 20.07 | a=3.1282 | 12.03 | 0.006995 |
| | Ti | 0.53 | a=3.3210 | 21.34 | 0.001654 |

Profilograms results indicate that the average surface roughness is $R_a$ = 0.089 m, and it changes after plating. **Figure 5** show AFM images of the surface topography of the coating on the basis of a series 4 of systems (Ti-Zr-Cr-Nb)N.

A comparison of the data shows that the change in the roughness of the coating (Ti-Zr-Cr-Nb) N is directly dependent on the pressure of the reaction of nitrogen dioxide and mixing capabilities. At a pressure of $P_N$ = 0.7 Pa, a more uniform surface is obtained by coating, with pronounced drip inclusions of small sizes. At a pressure of $P_N$ = 0.3 Pa, the coating formed on the surface is not a completely melted compound of elements Ti, Zr, Cr, Nb, and nitrogen.

Results of adhesion-cohesive strength and resistance to scratching studies are shown in **Figures 7, 8,** and **9**. Changing the coefficient of friction values and acoustic emission signals by increasing the scribing load **(Figure 7)** determines the characteristic values of the critical loads $L_C$: $L_{C1}$ – the firstappearance of chevron cracks at the bottom, and diagonal cracks on the

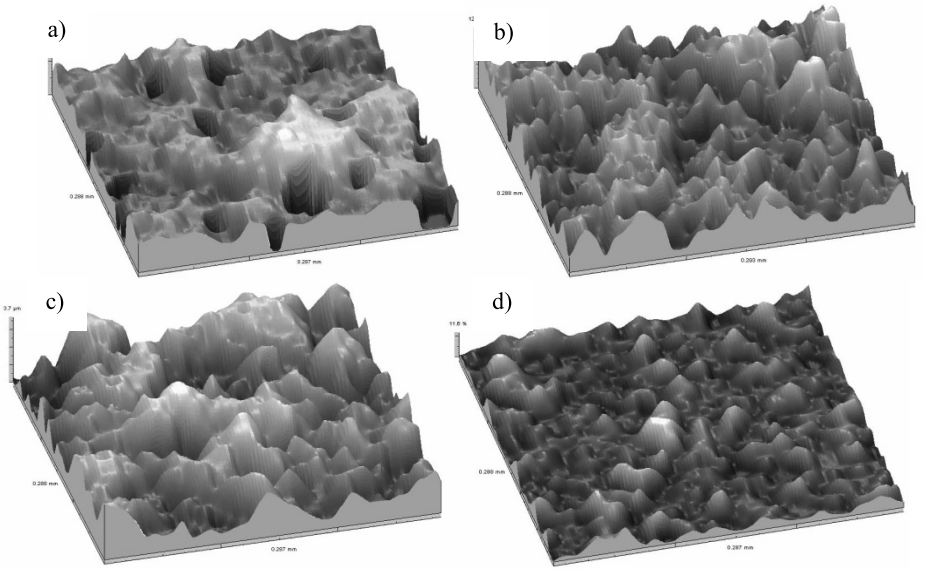


**Fig. 5. Dimensional AFM image of the surface coating (Ti-Zr-Cr-Nb)N: (a) $P_N$ = 0.3 Pa, $U_b$ = -100 V, $R_a$ = 1.69 mm (Series 1), (b) $P_N$ = 0.7 Pa, $U_b$ = -100V, $R_a$ = 1.83 mm (Series 2), (c) $P_N$ = 0.3 Pa, $U_b$ = -200 V, $R_a$ = 1.88 mm (Series 3), and (d) $P_N$ = 0.7 Pa, $U_b$ = -200 V, $R_a$ = 1.55 mm (Series 4)**

Rys. 5. Trójwymiarowy obraz AFM powierzchni powłoki (Ti-Zr-Cr-Nb)N: (a) $P_N$ = 0,3 Pa, $U_b$ = -100 V, $R_a$ = 1,69 mm (Seria 1), (b) $P_N$ = 0,7 Pa, $U_b$ = -100V, $R_a$ = 1,83 mm (Seria 2), (c) $P_N$ = 0,3 Pa, $U_b$ = -200 V, $R_a$ = 1,88 mm (Seria 3) oraz (d) $P_N$ = 0,7 Pa, $U_b$ = -200 V, $R_a$ = 1,55 mm (Seria 4)

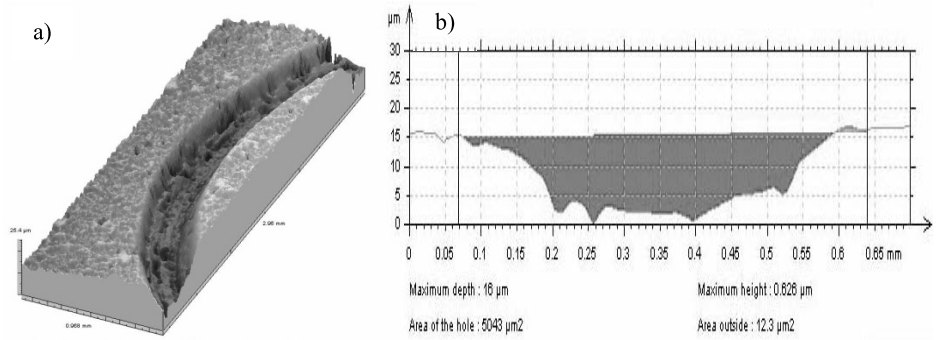


**Fig. 6. A dimensional AFM image (a) and profilogram ( b) of the coating surface of the friction track. (coating (Ti-Zr-Cr-Nb)N, $P_N$ nitrogen at a pressure of 0.3 Pa and $U_b$ = -200 V)**

Rys. 6. Trójwymiarowy obraz AFM (a) i profilogram (b) ścieżki tarcia na powierzchni powłoki (powłoka (Ti-Zr-Cr-Nb)N, ciśnienie azotu $P_N$ = 0,3 Pa i $U_b$ = -200 V)

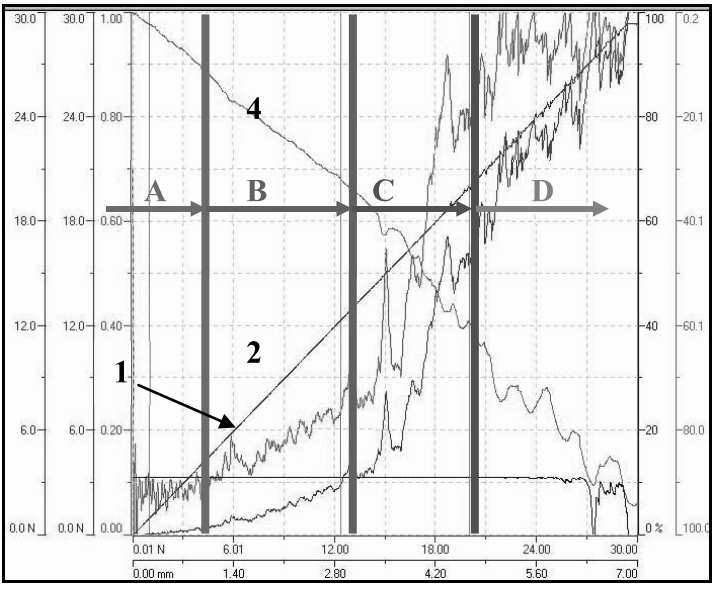


A – zone 1, $L_{C1}$; B – zone 2, $L_{C2}$; C – zone 3, $L_{C3}$; D– zone 4, $L_{C4:}$

**Fig. 7. The results of measurements of mechanical characteristics of the applied load during scratch testing of the coating (Ti-Zr-Cr-Nb)N, obtained by $P_N$ = 0.7 Pa and $U_b$ =-100 V; 1 – coefficient of friction (µ); 2 – normal load ($F_N$); 3 – acoustic emission ($A_E$); |4 – the depth of penetration ($P_h$)**

Rys. 7. Wyniki pomiarów charakterystyk mechanicznych podczas testu zarysowania powłoki(Ti-Zr-Cr-Nb)N wytworzonej przy $P_N$ = 0,7 Pa oraz $U_b$ =-100 V: 1 – współczynnik tarcia (µ); 2 – obciążenie normalne ($F_N$); 3 – sygnał emisji akustycznej ($A_E$); 4 – głębokość penetracji ($P_h$)

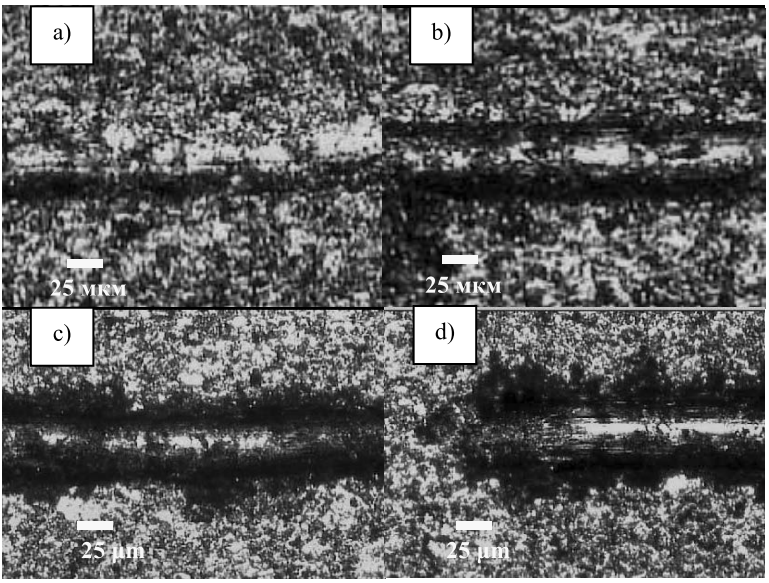


*a* – zone 1, *b* – zone 2, *c* – zone 3, *d* – zone 4

**Fig. 8. Photomicrographs of the diamond indenter contact area of coatings based on (Ti-Zr-Cr-Nb)N, obtained by $P_N$ = 0.7 Pa and $U_b$ = -100 V**

Rys. 8. Mikrofotografie obszaru styku diamentowego wgłębnika na powierzchni powłoki (Ti-Zr-Cr-Nb)N wytworzonej przy $P_N$ = 0,7 Pa oraz $U_b$ = -100 V

boundaries; $L_{C2}$ – forming a plurality of chevron cracks in the bottom of the crack and peel local coverage, chevron formation of cracks at the bottom of scratches; $L_{C3}$ – cohesively-coating adhesion failure; $L_{C4}$ – plastic coating abrasion. During the test, the adhesive strength was taken as the $L_{C4}$ critical load value of the abrasion resistance of the coating.

In accordance with these criteria, the process of the destruction of the coating evidenced by the scratching by indenter can be divided into four stages. At the load range of F = 0.01 to 5.50 N there is monotonic penetration into the coating, and the coefficient of friction increases significantly, and the acoustic emission signal is kept unchanged. At the load of F = 6.01N, the indenter is completely immersed in the coating, and the friction coefficient is 0.25. When the load increases (F = 12,01 – 30 N) takes place before the material squeezing the indenter in the form of hillocks, and increase the penetration depth of the indenter.

Comparative analysis demonstrates that coating abraded but did not peel off during scratch tests. The breaking of the cohesive mechanism is associated with plastic deformation and the formation of fatigue cracks in the coating material **(Fig. 9)**.

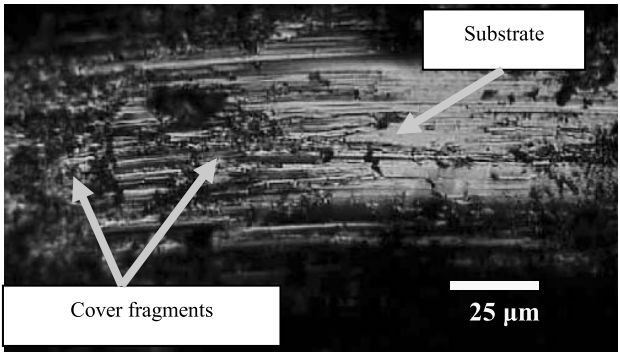


**Fig. 9. Image of surviving fragments of coating covering the bottom of the crack after exposure to the diamond indenter**

Rys. 9. Obraz zachowanych fragmentów powłoki pokrywających dno zarysowania po przejściu wgłębnika diamentowego po teście zarysowania

Micro-hardness testing is known to be the most versatile option, that allows the rapid evaluation of the mechanical properties of the coating. The results of such measurements for coatings (Ti-Zr-Cr-Nb)N are shown in **Table 5**. As can be seen, the maximum hardness HV = 43.93 GPa is achieved at a pressure of reaction gas $P_N$ = 0.7 Pa and the bias potential of -200 V = $U_b$.

**Table 5. The results of measurements of hardness of coating (Ti-Zr-Cr-Nb)N**

Tabela 5. Wyniki pomiarów twardości powłok (Ti-Zr-Cr-Nb)N

| Number of samples (series) | Hardness, $HV_{0.1}$GPa |
|---|---|
| 1 | 30.93 |
| 2 | 34.78 |
| 3 | 38.86 |
| 4 | 43.93 |

Thus, the experimental and theoretical research results represent a new step in the task of creating a protective coating on the basis of multi-component systems (Ti-Zr-Cr-Nb)N, producing structural and phase characteristics, that make it possible to increase the performance of different products, operating at high temperatures with a, load and rate of wear. The hardness of the resulting coatings (Ti-Zr-Cr-Nb)N is changed, depending on the deposition conditions of: pressure of the reaction gas $P_N$ and offset potential $U_b$.

## CONCLUSIONS

By vacuum-arc deposition integrally-molded cathode reaction in a nitrogen gas atmosphere prepared multicomponent coating system (Ti-Zr-Cr-Nb) N. Experimental and theoretical studies show that the coatings obtained by the

selected deposition parameters-, have a coating thickness of 6.2 microns. The highest microhardness (43.93 GPa), and wear resistances were obtained by coatings produced with a maximum nitrogen pressure. For these coatings, the (Ti-Zr-Cr-Nb)N phase typically forms a nitride TiN. The coatings are characterized by good adhesive strength and a cohesive mechanism for the break during the tests. On physical and mechanical characteristics of the resulting coating system (Ti-Zr-Cr-Nb)N are promising for the use of this type of coating.

## REFERENCES


1. Kavaleiro A., de Hossona D. Nanostruturnye pokrytia – 2011. – M.: Tehnosfera, – 792 s.
2. Musil J., Hard and superhard nanocomposite coatings//Surf. Coat.Tehnol. – 2000. –Vol. 125. – P. 322–330.
3. Andrievskii R.A., Sverhtverdye nanostrukturnye materialy na osnove tugoplavkih soedinenii//Zh. funkc. mater. – 2007. – T.1, № 4. – s. 129–133.
4. Azarenkov N.A., Beresnev V.M., Pogrebnjak A.D., Malikov L.V., Turbin P.V., Nanomaterialy, nanopokrytia, nanotehnologii: uchebn. posobie // Harkov: HNU im. V.N. Karazina, 2009. – 209 s.
5. Pogrebnjak A.D., Shpak A.P., Azarenkov N.A., Beresnev V.M., Struktura i svoistva tverdyh I sverhtverdyh nanokompozitnyh pokrytii // UFN. – 2009. – T. 179, № 1. – s. 35–64.
6. Moshkov V.Ju., Korotaev A.D., Pinjin Ju.P., Ovchinnikov S.V., O prirode sverhtverdosti nanokompozitnyh pokrytii na osnove TiN// sb. tezisov XVII Mejdunarodnoi konferencii., Samara. – 2009. – S. 265.
7. Andreev A.A., Sablev V.P., Shulaev V.M., Grigorev S.N., Vakuumno-dugovye ustroistva I pokrytia – Harkov: NNC “HFTI”, 2005. – 236 s.
8. Beresnev V.M., Tolok V.T., Shvec O.M. I dr., Mikro-nanosloinye pokrytia sformirovannye metodom vakuumno-dugovogo osajdenia s ispolzovaniem VC-razriada // FIP. – 2006. – T. 4, № 1–2. – S. 93–97.
9. Anders A. (Ed.). Handbook of Plasma Immersion Ion Implantation and Deposition //John Wiley & Sons, New York. – 2000. – P. 435.
10. Metody i sredstva uprocnenia poverhnostey detaley mashin koncentrirovannymi potokami energii / Pod red. A.P. Gusenkova M.: Nauka. 1992. – 406 S.
11. Pelletier J., Plasma-based ion implantation and deposition: A review of Physics, Technology, and Application / Pelletier J., Anders A. // IEEE Transactions on Plasma Science. – 2005. – Vol. 33, No. 6 – P. 1944–1959.
12. Morris D.G., Mechanical behaviour of nanocrystalline materials // Material science foundation. Trans. tech. publication LVD Switzerland, Germany, UK, USA – 1998. – Vol. 2. – P. 1–84.

**Streszczenie**

**W opracowaniu przedstawiono wyniki badań wieloskładnikowych powłok ceramicznych (Ti-Zr-Cr-Nb)N, wytworzonych z wykorzystaniem metody łukowo-próżniowej. Badania teoretyczne i doświadczalne wykazują, że skład chemiczny, mikrostruktura oraz właściwości mechaniczne powłok związane są ściśle z parametrami osadzania (ciśnienia roboczego gazu i potencjału polaryzacji na podłożu). Mikrostruktury powłok badano za pomocą skaningowego mikroskopu elektronowego (SEM) wyposażonego w przystawki do mikroanalizy dyspersji energii i dyfrakcji rentgenowskiej (XRD). Przeprowadzona analiza fazowa powłok (Ti-Zr-Cr-Nb)N wykazała występowanie faz TiN, $NbTiN_2$, ZrTiNb, ZrNb, TiCr oraz α-Ti. Zmierzona grubość powłok osiągała wartość 6,8 μm natomiast największa ich twardość H = 43,7GPa. Badane były również właściwości tribologiczne powłok (metoda ball-on-disc) i mechaniczne (test zarysowania). Wyniki przeprowadzonych analiz wieloskładnikowych powłok ceramicznych (Ti-Zr-Cr-Nb)N są bardzo obiecujące i wykazują, że mogą być one stosowane jako powłoki ochronne dla narzędzi skrawających oraz w materiałach strukturalnych.**